

# Thieno[3,2-*b*]thiophene oligomers and their applications as p-type organic semiconductors†

Moawia O. Ahmed,<sup>a</sup> Chunmei Wang,<sup>a</sup> Peisi Keg,<sup>a</sup> Wojciech Pisula,<sup>b</sup> Yeng-Meng Lam,<sup>a</sup> Beng S. Ong,<sup>c</sup> Siu-Choon Ng,<sup>d</sup> Zhi-Kuan Chen<sup>\*c</sup> and Subodh G. Mhaisalkar<sup>\*a</sup>

Received 16th January 2009, Accepted 26th February 2009

First published as an Advance Article on the web 3rd April 2009

DOI: 10.1039/b900979e

This study describes the synthesis, characterization and electronic properties of a novel series of soluble thieno[3,2-*b*]thiophene oligomers (**1a** and **b** and **2a** and **b**) for thin film transistor (TFT) applications. All the compounds were synthesized in high yield using Pd-catalyzed Stille or Suzuki coupling reactions and were substituted by two dodecyl groups at the 3- or 4-position of the thiophene unit to ensure the solubility for facile device fabrication. Aryl units such as phenyl and naphthyl were used for ‘end-capping’ to provide stability against oxidation. The design of these materials has focused on their self-assembly and solution processability. All the compounds have been characterized by <sup>1</sup>H, <sup>13</sup>C NMR, and elemental analysis. Their electronic and optical properties were investigated using UV-Vis and photoluminescence spectroscopy, cyclic voltammetry, thermal gravimetric analysis (TGA), and differential scanning calorimetry (DSC). High-resolution STM images of **1a** and **2a** adsorbed on HOPG revealed highly ordered self-organized domains. Two-dimensional wide-angle X-ray scattering (2D-WAXS) was used to study the solid state packing of **1a** and **2a**. Top-contact OTFT devices from **1a** were prepared by spin coating and showed promising behaviour with mobilities up to  $3.11 \times 10^{-2} \text{ cm}^2 \text{ V}^{-1} \text{ s}^{-1}$  and on/off ratios up to  $10^4$ .

## Introduction

Organic thin film transistors (OTFTs) have recently received considerable attention due to their ease of fabrication by solution techniques which offer the potential for roll-to-roll printing and thus for low cost high volume manufacturing processes.<sup>1–4</sup> In the past two decades, a great variety of organic semiconductors have been developed and explored. Among them, thiophene or fused thiophene, in particular thieno[3,2-*b*]thiophene based oligomeric and polymeric materials, are the widely investigated materials for OTFTs due to their high mobility.<sup>5–11</sup> McCulloch *et al.* have demonstrated high mobility poly[2,5-bis(3-alkylthiophen-2-yl)-thieno(3,2-*b*)thiophene] semiconductors, with mobilities of up to  $0.6 \text{ cm}^2 \text{ V}^{-1} \text{ s}^{-1}$ .<sup>12</sup> While Ong and coworkers reported a poly[2,5-bis(2-thienyl)-3,6-dipentadecylthieno(3,2-*b*)thiophene] that showed a high mobility of  $0.25 \text{ cm}^2 \text{ V}^{-1} \text{ s}^{-1}$  under ambient conditions.<sup>16</sup> Recently, Tokiyoshi and Shizuo have reported highly crystalline thin films of liquid-crystalline poly[2,5-bis(3-tetradecylthiophene-2-yl)-thieno(3,2-*b*)thiophene] with mobilities of up to  $0.44 \text{ cm}^2 \text{ V}^{-1} \text{ s}^{-1}$ .<sup>8</sup> However, thieno[3,2-*b*]thiophene based polymers show insufficient solubility at room temperature, which

makes it very challenging for device fabrication through a solution process.<sup>13</sup> Their oligomeric counterparts are potentially advantageous over the polymer analogs because of their good solution processability, facile synthesis and purification, and well-defined structure.<sup>14</sup> In addition, these low molecular weight semiconductors can be deposited by both vacuum sublimation and solution process techniques. One of the main issues with most oligomeric semiconductors containing thiophene or thienothienophene building blocks is the rapid degradation of their TFT devices due to the relatively low ionisation potentials.<sup>3</sup> Thus, it is an aim of the present work to provide new organic materials for use as semiconductors, which will allow straightforward up-scaling due to a well-designed synthetic route, with good air and thermal stability. The work reported here also focuses on materials that are easily processable and can be readily deposited by a solution process method. For this purpose, four oligomeric compounds (**1a** and **b** and **2a** and **b**) using thieno[3,2-*b*]thiophene as the building blocks (see Scheme 1 and 2) have been designed and synthesized. Two alkyl chains were introduced at the 3 or 4-position of the thiophene ring to ensure a better solubility for easier device fabrication. Aryl units such as phenyl and naphthyl groups were used as ‘end-cap’ substituents to enhance material/device stability against oxidation. The devices derived from oligothiophenes, end-capped with an aryl unit, not only show very high mobilities (up to  $0.4 \text{ cm}^2 \text{ V}^{-1} \text{ s}^{-1}$ ) and high on/off current ratios ( $I_{\text{on}}/I_{\text{off}}$  up to  $10^5$ ) but are also found to be stable in air and under ambient illumination.<sup>14a</sup>

Herein we report the synthesis and characterization of a series of solution processable small compounds (**1a** and **b** and **2a** and **b**) based on thieno[3,2-*b*]thiophene, for TFT applications. To investigate their solid state packing, we performed

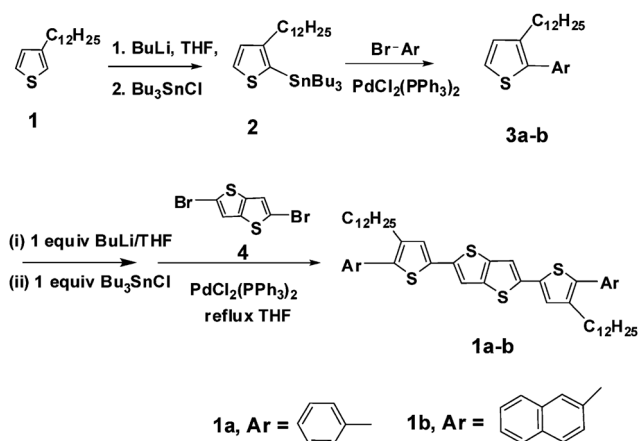
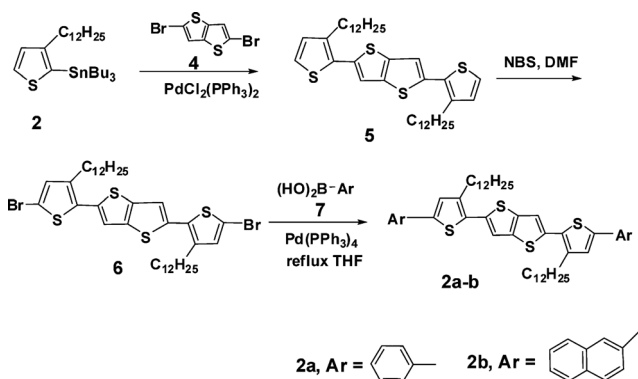
<sup>a</sup>School of Materials Science and Engineering, Nanyang Technological University, 50 Nanyang Avenue, 639798 Singapore. E-mail: subodh@ntu.edu.sg

<sup>b</sup>Max Planck Institute for Polymer Research, Ackermannweg 10, 55128 Mainz, Germany

<sup>c</sup>Institute of Materials Research and Engineering (IMRE), 3 Research Link, 117602 Singapore. E-mail: zk-chen@imre.a-star.edu.sg

<sup>d</sup>Division of Chemical and Biomolecular Engineering, Nanyang Technological University, 637459 Singapore

† Electronic supplementary information (ESI) available: MALDI-TOF and DSC spectra. See DOI: 10.1039/b900979e

Scheme 1 Synthesis of oligomers **1a** and **b**.Scheme 2 Synthesis of oligomers **2a** and **b**.

two-dimensional wide-angle X-ray scattering (2D-WAXS) studies on two compounds (**1a** and **2a**).

## Results and discussion

### Synthesis

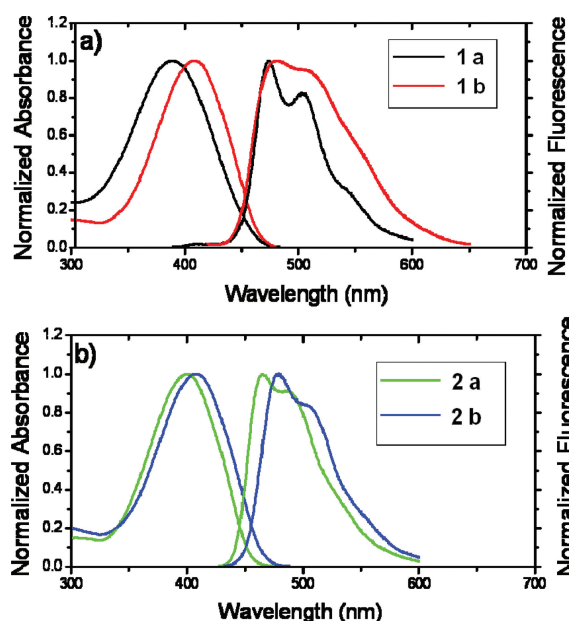
The syntheses of compounds **1a** and **b** and **2a** and **b** were conveniently achieved as outlined in Scheme 1 and 2. Compounds **1a** and **b** were synthesized in good yields by utilizing a one-pot Stille coupling<sup>15</sup> of 2,5-dibromothiopheno[3,2-*b*]thiophene **4** and the corresponding freshly prepared tri-*n*-butylstannyl derivatives of **3a** [tributyl(4-dodecyl-5-phenyl-thiophen-2-yl)-stannane] for **1a** and **3b** [tributyl(4-dodecyl-5-naphth-2-yl)-thiophen-2-yl)stannane] for **1b**, in the presence of PdCl<sub>2</sub>(PPh<sub>3</sub>)<sub>2</sub>, under reflux in THF (Scheme 1). Compounds **2a–b** were synthesized by the Suzuki coupling of 2,5-bis(5-bromo-3-dodecylthiophen-2-yl)thiophene **6** and the appropriate aryl boronic acid **7** [phenyl boronic acid (**2a**) or 2-naphthyl boronic acid (**2b**)] using Pd(PPh<sub>3</sub>)<sub>4</sub> under reflux in THF in good yields (Scheme 2). All the compounds are soluble in organic solvents such as CHCl<sub>3</sub>, toluene, THF, and can be easily purified by column chromatography and recrystallization. The structures of **1a** and **b** and **2a–b** were characterized by <sup>1</sup>H, <sup>13</sup>C NMR, elemental analysis and MALDI-TOF mass spectrometry. The results were consistent with the predicted chemical structures.

The optical and electrochemical properties of **1a** and **b** and **2a** and **b** were examined by UV-Vis absorption spectroscopy, fluorimetry and cyclic voltammetry. The results are summarized in Table 1. The absorption and emission spectra of **1a** and **b** and **2a** and **b** in dilute THF are depicted in Fig. 1. All the compounds show strong absorption and emission peaks in the 350–420 nm and 470–480 nm ranges respectively. As expected, the absorption and emission maxima of **1b** and **2b** with naphthalene units are red-shifted compared to that of **1a** and **2a** with phenyl units. The HOMO–LUMO gaps estimated from the absorption edges are 2.71 eV for **1a**, 2.66 eV for **1b**, 2.73 eV for **2a** and 2.67 eV for **2b**. The oxidation potentials measured by cyclic voltammetry (CV) (Fig. 2) of **1a** and **b** and **2a** and **b** are 0.88, 0.80, 0.84 and 0.81 V (reference to SCE) respectively, from which the HOMO levels were calculated as shown in Table 1. The HOMO levels of all compounds range from –5.20 eV to –5.28 eV, which is significantly lower than most of the thiophene based oligomers and

Table 1 Photophysical properties of **1a** and **b** and **2a** and **b**

Compound	$T_m/^\circ\text{C}^a$	$T_d/^\circ\text{C}^b$	UV-Vis $\lambda_{\text{max}}/\text{nm}^c$	PL $\lambda_{\text{max}}/\text{nm}^c$	HOMO–LUMO (band gap)/ eV <sup>d</sup>
<b>1a</b>	124	360	389	474	–5.25/–2.54 (2.71)
<b>1b</b>	114	395	409	480	–5.20/–2.61 (2.66)
<b>2a</b>	117	397	401	465	–5.28/–2.55 (2.73)
<b>2b</b>	118	400	407	478	–5.21/–2.54 (2.67)

<sup>a</sup> Obtained from DSC measurement. <sup>b</sup> Obtained from TGA measurement. <sup>c</sup> Measured as a THF solution. <sup>d</sup> Calculated from CV and UV-Vis absorption spectra band edges.

Fig. 1 UV-Vis and PL spectra of (a) **1a** and **b**, (b) **2a** and **b**.

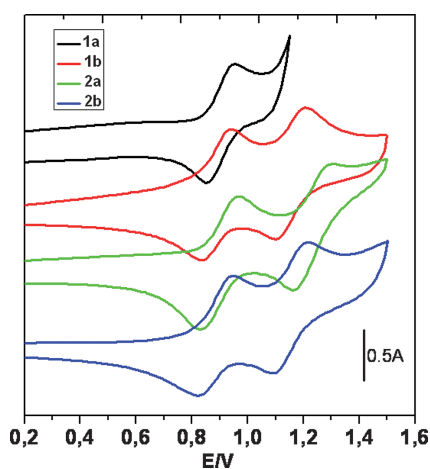


Fig. 2 Cyclic voltammograms of **1a** and **b** and **2a** and **b**.

polymers, indicating higher stabilities of **1a** and **b** and **2a** and **b**.<sup>3,4,16</sup> In addition, the HOMO levels of all the compounds match well with the workfunction of metallic gold ( $-5.1$  eV) and efficient hole charge injection between the electrode and the semiconductor is anticipated.<sup>17</sup>

The thermal behaviour of compounds **1a** and **b** and **2a** and **b** was determined by thermal gravimetric analysis (TGA) and differential scanning calorimetry (DSC) (results are summarized in Table 1). All the compounds demonstrated excellent thermal stabilities, with decomposition temperatures above  $360$  °C and melting points higher than  $110$  °C. Fig. 3 presents the DSC traces for **1a** and **2a** respectively. It is interesting to note that at the same cooling rate of  $10$  °C  $\text{min}^{-1}$ , only **1a** undergoes crystallization, while **2a** remains amorphous. Therefore, during the second heating cycle **2a** reveals two cold-crystallization peaks. The variation of the thermal properties might indicate a different influence of the side chains on the packing.

To further understand the two-dimensional self-organization of the compounds, the adsorption of **1a** and **2a** on highly ordered pyrolytic graphite (HOPG) was investigated using scanning tunnelling microscopy (STM) in the solid–liquid interface.<sup>18</sup> Due to the rough surface conditions of  $\text{SiO}_2$  substrate surfaces, it was not possible to conduct STM investigations on those surfaces; hence an alternative substrate was used. HOPG substrates have been widely used as surfaces for the study of molecular

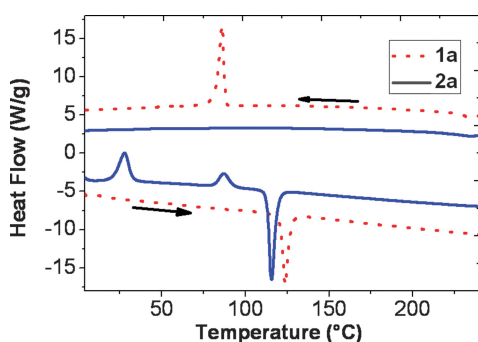


Fig. 3 DSC scans for **1a** and **2a** at a rate of  $10$  °C  $\text{min}^{-1}$ . The heating-cooling directions are indicated by the arrows.

adsorption due to their atomically flat surface and chemical inertness. Adsorption studies of conjugated polythiophenes, oligothiophenes and anthracene molecules on HOPG substrates have been found to correlate successfully with their three-dimensional crystal packings, X-ray diffraction studies and device performances.<sup>19</sup> It has also been found that molecules typically possess the same molecular order of the two-dimensional adsorbed monolayer on the HOPG surface as one layer of its three-dimensional crystal. In addition to that, previous studies using STM and AFM have also shown the close relationship between the organization of polyquaterthiophenes on HOPG surfaces and  $\text{SiO}_2$  surfaces.<sup>19a</sup>

On deposition, both compounds appear to self-organize into highly ordered domains extending over  $500$  nm with a long range order of lamellar rows (Fig. 4). Due to the electron rich system concentrated at the main chain backbone of the thienothiophene molecule, the backbones tend to appear as brighter areas from the higher tunnelling currents. Alkyl chains thus appear as spots, where only half the number of  $-\text{CH}_2$  groups from the alkyl chains are visible, which is typically the case for alkyl chain adsorption onto the HOPG surfaces, arising from the commensurability between the alkyl chains and graphite sheet.<sup>20</sup>

Alkylated oligothiophenes have been generally observed to adsorb flatly on HOPG surfaces, with the alkyl chains spread out and extended, parallel to the substrate surface.<sup>21</sup> These alkyl chains were also observed to interdigitate due to van der Waals interactions, hence forming neat rows of organized lamellae. Visible alkyl chain interdigitation from adjacent rows of compounds **1a** and **2a** were observed in both images. Despite different substituents sites, both compounds appear to possess a similar packing order with slight differences in the unit cell dimensions. The 2D unit cell parameters measured by STM for **1a** are  $a = 1.4 \pm 0.1$  nm;  $b = 2.5 \pm 0.1$  nm;  $\alpha = 79 \pm 2^\circ$  and for **2a** are  $a = 1.4 \pm 0.1$  nm;  $b = 2.9 \pm 0.1$  nm;  $\alpha = 81 \pm 2^\circ$ . It can be inferred that the compounds lie seemingly flat and planar on the surfaces upon adsorption.

Since supramolecular order is one key parameter for the performance of organic semiconductors in devices, the organization of **1a** and **2a** was investigated by using two-dimensional wide-angle X-ray scattering. The samples were prepared by filament extrusion<sup>22</sup> below their melting points at a temperature of  $100$  °C. Fig. 5a shows a characteristic pattern for **2a** recorded

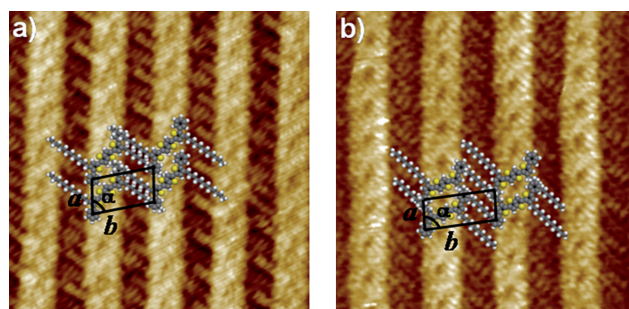
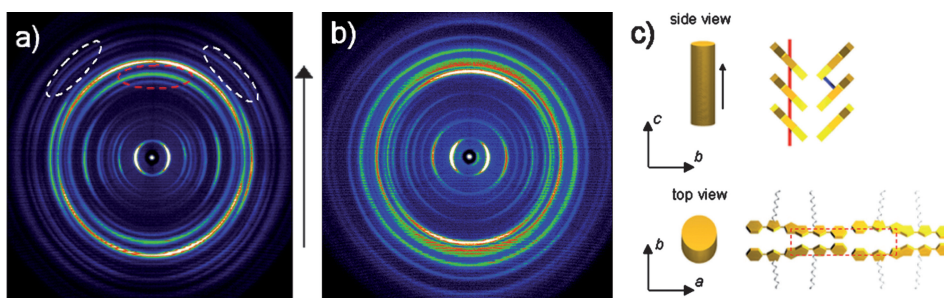


Fig. 4 Typical constant current STM images of self-organized monolayers of (a) **1a** adsorbed at the *n*-tetradecane–HOPG interface ( $12$  nm  $\times$   $12$  nm;  $I_t = 75$  pA;  $V_t = 78$  mV) and (b) **2a** adsorbed at the *n*-tetradecane–HOPG interface ( $12$  nm  $\times$   $12$  nm;  $I_t = 80$  pA;  $V_t = -200$  mV).



**Fig. 5** (a) 2D-WAXS pattern of **2a** at 30 °C (arrow indicates the extruded direction of the sample towards the detector, the white dashed circle marks reflections which are related to the  $\pi$ -stacking and the red circle corresponds to the intra-lamella spacing), (b) **1a** at 30 °C, and (c) schematic illustration of the supramolecular organization of **2a**. In the side view drawing, the red line corresponds the intra-lamella spacing of 0.48 nm oriented along the alignment direction, whereas the blue line represents the  $\pi$ -stacking distance of 45° tilted oligomers. The parameters  $a$  and  $b$  are randomly distributed around  $c$  which coincides with the fiber axis.

at 30 °C, whereby no change of the solid state superstructure was observed with the variation of temperature. In both cases, the 2D patterns indicate highly ordered structures, whereby the distribution of the scattering intensities implies a perpendicular orientation of the oligomers with their molecular planes to the fiber axis. The supramolecular organization in the extruded filament of **1a** is schematically illustrated in Fig. 5b. The first wide-angle meridional reflections related to a spacing of 0.48 nm are attributed to perpendicularly aligned oligomers which are packed on top of each other due to  $\pi$ -stacking interactions forming a lamella superstructure. The  $\pi$ -stacking distance of 0.34 nm is represented by additional off-meridional reflections which appear at an angle of 45° towards the meridional pattern plane. This angle is in agreement with the molecular tilting of **2a** towards the lamella axis ( $c$  axis) and to the herringbone single crystal structure of thieno[3,2-*b*]thiophene based molecules reported previously.<sup>3</sup> An identical intra-lamella organization has been determined for **1a**. The two other axes of the unit cell,  $a$  and  $b$ , are randomly oriented around the fiber direction leading to reflections in the equatorial plane of the 2D pattern. For both cases, an orthorhombic unit cell was derived from the positions of the reflections with lattice parameters of  $a = 2.12$  nm and  $b = 0.85$  nm for **1a** and  $a = 2.23$  nm and  $b = 0.92$  nm for **2a**. These packing parameters cannot be compared directly to the organization of thienothiophene based polymers possessing the same dodecyl alkyl substituents.<sup>23</sup> In our case, the  $a$  parameter is in agreement with the molecular length of the oligomers, while  $b$  corresponds to the distance between lamellae.

These lamella structures are formed due to  $\pi$ -stacking interactions of the aromatic rods and the local phase separation between the flexible alkyl side chains and the rigid rods. The

higher the steric hindrance of the alkyl substituents, the more pronounced the phase separation and the more improved the macroscopic alignment in the extruded filament. Apparently, in the case of **2a**, the side chains possess slightly larger steric hindrance due to their substitution position, softening the material and resulting in better alignment during mechanical shearing in comparison to **1a**. The different roles of the side chains can be clearly observed in the thermal behaviour and crystallization behaviour as discussed above (Fig. 3). DSC revealed that during cooling **1a** crystallized at a temperature of 75 °C, while the crystallization of **2a** was suppressed at the same cooling rate. This verifies the slightly larger steric influence of the side chains for **2a**. During the second heating two exothermic peaks appeared which were assigned to a cold-crystallization of **2a**. Furthermore, the melting temperature of **1a** was higher (124 °C) in comparison to **2a** (117 °C) also indicating the stronger interactions of the **1a** molecules.

To obtain further information about the supramolecular organization of the compounds, the phases were investigated using polarized optical microscopy (POM). Surprisingly, in both cases well-ordered spherulites nucleated randomly over the whole sample during the cooling of the materials from the isotropic state (Fig. 6). The spherulites revealed high anisotropy and therefore coherent long range order. This was expressed by the Maltese cross, where the isogyres followed the extinction of the analyzer/polarizer direction, indicating a radial alignment of the assemblies from the center. Using an  $\alpha$ -plate and analyzing the red–blue distributions in the optical spherulite image, it was possible to determine that the spherulites are optically negative (Fig. 6b). The refractive index parallel to the radial direction is smaller than that perpendicular to it. An

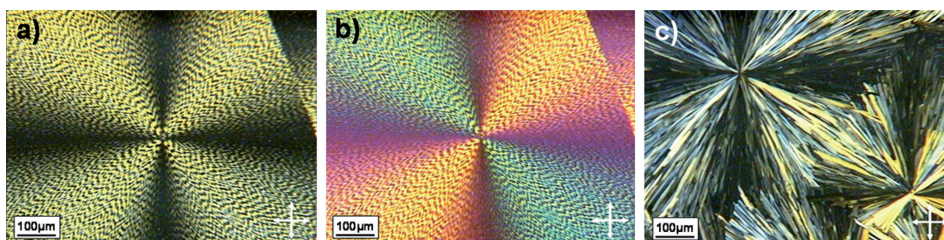


**Fig. 6** (a) POM images of **2a** between cross-polarizers at 25 °C crystallized at a cooling rate of 25 °C min<sup>-1</sup>, (b) with an  $\alpha$ -plate and (c) at 90 °C.

identical optical behaviour of such optically negative spherulitic domains was also observed for small molecules organized in columnar systems.<sup>24</sup> The analysis of these optical textures of **1a** and **2a** suggests that the oligomers assemble in lamella superstructures which in turn might be oriented macroscopically in the spherulite growth direction with an edge-on arrangement of the molecules. The observed domains of both oligomers exceeded several hundreds of micrometres, whereby the spherulite size and morphology was dependent on the cooling rate. Upon closer inspection of the spherulites of **2a**, a macroscopic periodicity along the radius was discovered (Fig. 6). The periodic contrast, due to birefringent effects, appears on single fibrous structures, suggesting a helical twist of crystallites within the fibers. It is known that extinction occurred in such banded spherulites when the optical axis of crystallites coincided with the polarization plane.<sup>25</sup> In the case of **2a**, the macroscopic helical pitch was *ca.* 25  $\mu\text{m}$ . However, after heating the film of **2a** over the second phase transition observed in the DSC scan, the morphology changed to a more crystalline texture and the helical features disappeared (Fig. 6c).

### OTFT characteristics

Fig. 7 shows the typical FET electrical characteristics of a bottom-contact TFT (Fig. 7a) and a top-contact TFT (Fig. 7b) made from **1a** spin coated from toluene under air. Annealing took place in a vacuum oven at a temperature of 70  $^{\circ}\text{C}$  for 1 h, followed by 100  $^{\circ}\text{C}$  for 20 min. It was then cooled under vacuum overnight to ensure molecular ordering. The bottom-contact device has a saturation charge carrier mobility of  $5.0 \times 10^{-4} \text{ cm}^2 \text{ V}^{-1} \text{ s}^{-1}$ , a subthreshold slope of 0.98 V decade<sup>-1</sup>, and an on/off ratio of  $2 \times 10^3$ . Comparatively, the top-contact device outperforms the bottom-contact TFTs, with a higher saturation mobility of  $3.1 \times 10^{-2} \text{ cm}^2 \text{ V}^{-1} \text{ s}^{-1}$ , a lower subthreshold slope of 0.4 V decade<sup>-1</sup>, and a higher on/off ratio of  $4.5 \times 10^4$ . The better performance of top-contact organic TFT devices is typically attributed to small charge injection areas and poor ordering of the organic semiconductor on the electrodes in the bottom-contact geometry.<sup>26</sup> In comparison to the solution processed devices, bottom-contact OTFT made from **1a** deposited by thermal evaporation shows a mobility of  $1.4 \times 10^{-4} \text{ cm}^2 \text{ V}^{-1} \text{ s}^{-1}$  with a subthreshold slope of 1.1 V decade<sup>-1</sup> and an on/off ratio of  $2.5 \times 10^3$  (Fig. S7, ESI<sup>†</sup>).

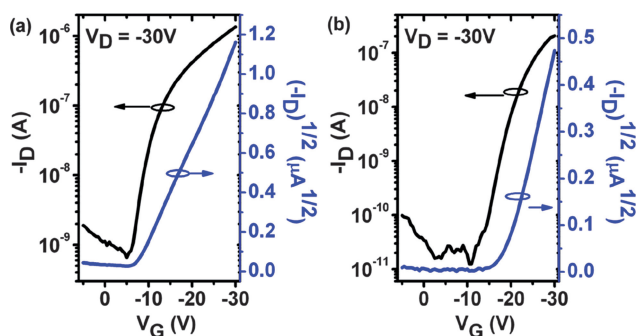


**Fig. 7** Transfer characteristics of **1a** for (a) a bottom-contact device and (b) a top-contact device.

### Conclusion

In summary, we have successfully synthesized a series of new organic semiconductors. The HOMO energy levels of all the materials are in the range of  $-5.20$  to  $-5.28 \text{ eV}$ , which match well with the work function of the gold electrodes, favoring the charge injection of holes. This study indicates that combining thieno[3,2-*b*]thiophene, thiophene and phenyl units in the conjugated compound is a promising approach for the creation of new stable semiconducting materials with good device performance. The presence of long alkyl chains in such compounds improves their solubilities as well as their molecular ordering, thus positively influencing their semiconducting properties. The thermal analyses as well as the electrochemical measurement data indicated better thermal and oxidation stability of the designed materials. Furthermore, we found that the OTFT devices based on compound **1a** have a high stability in air and exhibit excellent field-effect performances, with a mobility as high as  $3.1 \times 10^{-2} \text{ cm}^2 \text{ V}^{-1} \text{ s}^{-1}$  for a top-contact OTFT made by spin coating under normal air and  $1.4 \times 10^{-4} \text{ cm}^2 \text{ V}^{-1} \text{ s}^{-1}$ , for a bottom-contact OTFT deposited by thermal evaporation. Further studies of materials synthesis, device optimization and performance improvement are under way.

### Experimental section

#### General

Reactions and manipulations were performed using standard Schlenk techniques under an atmosphere of nitrogen or argon. Solvents were purified, dried, and distilled under an argon or nitrogen atmosphere prior to use. All new compounds were characterized by  $^1\text{H}$  and  $^{13}\text{C}$  NMR, MALDI-TOF mass spectrometry and elemental analysis.

#### Instruments

$^1\text{H}$  and  $^{13}\text{C}$  NMR spectra were collected on a Bruker DPX 400 MHz spectrometer with chemical shifts referenced to  $\text{CDCl}_3$ . Photoluminescence (PL) spectra were measured on a Perkin-Elmer (LS50B) fluorescence spectrometer. Thermal gravimetric analysis (TGA) was carried out using a TGA Q500 instrument (heating rate of 10  $^{\circ}\text{C} \text{ min}^{-1}$ ). Differential scanning calorimetry (DSC) was carried out under nitrogen on a DSC Q100 instrument (scanning rate of 10  $^{\circ}\text{C} \text{ min}^{-1}$ ). Cyclic voltammetry experiments were performed using an Autolab potentiostat (model PGSTAT30) by Echochimie. All CV measurements were recorded in dichloromethane with 0.1 M tetrabutylammonium hexafluorophosphate as the supporting electrolyte (scan rate of 100  $\text{mV} \text{ s}^{-1}$ ). The experiments were performed at room temperature with a conventional three electrode configuration consisting of a platinum wire working electrode, a gold counter electrode, and a Ag–AgCl in 3 M KCl reference electrode. Matrix assisted laser desorption/ionisation time-of-flight (MALDI-TOF) mass spectra were obtained on a Bruker Autoflex TOF/TOF instrument using dithranol as a matrix and silver trifluoroacetate as an ionizing salt when necessary.

The optical textures of the compound were investigated using a Zeiss microscope with polarizing filters equipped with a Hitachi KP-D50 Colour digital CCD camera. The samples were

sandwiched between two glass slides and then thermally treated on a Linkam hotstage regulated with a Linkam TMS 91 temperature controller.

The 2D-WAXS experiments were performed by means of a rotating anode (Rigaku 18 kW) X-ray beam with a pinhole collimation and a 2D Siemens detector. A double graphite monochromator for the Cu K $\alpha$  radiation ( $\lambda = 0.154$  nm) was used.

The samples were prepared by filament extrusion using a home-built mini-extruder. Therein, if necessary, the material is heated up to a phase at which it becomes plastically deformable and is extruded as 0.7 mm thin fiber by a constant-rate motion of the piston along the cylinder.

## Materials

NiCl<sub>2</sub>(dppp), 1-bromododecane, bromobenzene, tri-*n*-butyltin chloride, 3-bromothiophene, *tert*-butyllithium, lithium diisopropylamide (LDA), tetrakis(triphenylphosphine)palladium, PdCl<sub>2</sub>(PPh<sub>3</sub>)<sub>2</sub>, quinoline, 2-sulfonyl acetate, *N*-formylpiperidine, copper powder and *N*-bromosuccinimide (NBS), phenyl boronic acid and 2-naphthyl boronic acid, were all purchased from Aldrich. All reagents purchased commercially were used without further purification except for tetrahydrofuran (THF), which was dried over sodium–benzophenone.

## Synthesis

3-dodecylthiophene (**1**), tributyl(3-dodecylthiophen-2-yl)stannane (**2**), and 2,5-dibromothieno[3,2-*b*]thiophene (**4**) were prepared according to the procedures reported in the literature.<sup>27,28</sup>

### General method for the synthesis of **3**

3-Dodecylthiophene (5 g, 19.92 mmol) was dissolved in dry THF (40 mL) and cooled in an acetone–dry ice bath for 20 min. *tert*-Butyllithium (1.6 M) (12.5 mL, 19.92 mmol) was then added dropwise and the mixture was allowed to stir for 1 h. Tributyltin chloride (5.43 mL, 19.92 mmol) was then added dropwise and the mixture was allowed to warm to room temperature and stir for 1 h. Meanwhile, in a separate flask, PdCl<sub>2</sub>(PPh<sub>3</sub>)<sub>2</sub> (0.8 g, 0.56 mmol) was dissolved in THF (20 mL) and the appropriate bromoaryl (1-bromobenzene or 2-bromonaphthalene) (19.92 mmol) was added. The tributyl(3-dodecylthiophen-2-yl)stannane solution was transferred into the catalyst–bromoaryl solution and refluxed for 12 h. After the reaction was cooled to room temperature, water (250 mL) and hexane (100 mL) were added. The organic layer was separated, and the aqueous layer was extracted with dichloromethane. The organic layers were combined and dried over MgSO<sub>4</sub>, filtered and concentrated *in vacuo*. The crude product was purified by column chromatography on silica gel.

**3-Dodecyl-2-phenylthiophene (3a)** (90% yield): <sup>1</sup>H NMR (CDCl<sub>3</sub>, ppm)  $\delta$  7.63 (d,  $J = 7.6$  Hz, 2H), 7.39 (t,  $J = 7.6$  Hz, 2H), 7.29 (t,  $J = 7.6$  Hz, 1H), 7.19 (d,  $J = 4$  Hz, 1H), 6.89 (d,  $J = 4$  Hz, 1H), 2.65 (t,  $J = 7.6$  Hz, 2H), 1.71–1.65 (quintet, 2H), 1.38–1.32 (m, 18H), 0.94 (t,  $J = 7.2$  Hz, 3H); <sup>13</sup>C NMR (100 MHz, CDCl<sub>3</sub>, ppm):  $\delta$  144.65, 135.23, 129.94, 129.20, 128.80, 126.42, 125.20,

119.90, 32.46, 31.48, 31.16, 30.69, 30.21, 30.02, 29.88, 29.14, 23.21, 14.59. GC/MS  $m/z$ : 328.10 (M); calcd for C<sub>22</sub>H<sub>32</sub>S = 328

**3-Dodecyl-2-(naphth-2-yl)thiophene (3b)** (85% yield): <sup>1</sup>H NMR (CDCl<sub>3</sub>, ppm)  $\delta$  8.01 (s, 1H), 7.99–7.73 (m, 4H), 7.62–7.60 (m, 2H), 7.38 (d,  $J = 4.8$  Hz, 1H), 7.16 (d,  $J = 4.8$  Hz, 1H), 2.89 (t,  $J = 8$  Hz, 2H), 1.82–1.88 (quintet, 2H), 1.44–1.39 (m, 18 H), 1.07 (t,  $J = 6.8$  Hz, 3H). MALDI-TOF-MS (dithranol)  $m/z$ : 378.29 (M); calcd for C<sub>26</sub>H<sub>34</sub>S = 378.60

### General method for **1a** and **1b**

3-Dodecyl-2-phenylthiophene (**3a**) or 3-dodecyl-2-(naphth-2-yl)thiophene (**3b**) (10.67 mmol) was dissolved in dry THF (50 mL) and cooled in an acetone–dry ice bath for 20 min. *n*-Butyllithium, 1.6 M solution in hexanes, (6.68 mL, 10.67 mmol) was then added dropwise and the mixture was allowed to stir for 1 h. At this point the mixture was removed from the ice bath, allowed to warm to room temperature, and then returned to the ice bath. Tributyltin chloride (2.89 mL, 10.67 mmol) was then added dropwise and the mixture was allowed to warm to room temperature and stir for 1 h. The resulting tributyl(4-dodecyl-5-phenylthiophen-2-yl)stannane (**3a**) or tributyl(4-dodecyl-5-naphth-2-ylthiophen-2-yl)stannane (**3b**) solution was added by cannula under nitrogen to a solution of PdCl<sub>2</sub>(PPh<sub>3</sub>)<sub>2</sub> (0.19 g, 0.267 mmol) and 2,5-dibromothieno[3,2-*b*]thiophene (**4**) (1.59 g, 5.34 mmol) in THF (20 mL). The mixture was heated to reflux under argon for 20 h. The solution was then allowed to cool, quenched with water, and extracted with dichloromethane. The organic layer was separated and dried over MgSO<sub>4</sub>. The solvent was removed *via* rotary evaporation and the crude product was purified by column chromatography over silica gel and recrystallized from dichloromethane–ethanol.

**2,5-Bis(4-dodecyl-5-phenylthiophen-2-yl)thieno[3,2-*b*]thiophene (1a)** (3 g, 71% yield): <sup>1</sup>H NMR (CDCl<sub>3</sub>, ppm)  $\delta$  7.61 (d,  $J = 7.6$  Hz, 4H), 7.39 (t,  $J = 7.6$  Hz, 4H), 7.28 (t,  $J = 7.2$  Hz, 2H), 7.19 (s, 2H), 6.98 (s, 2H), 2.82 (t,  $J = 7.6$  Hz, 4H), 1.73–1.67 (m, 4H), 1.42–1.26 (overlapped peaks 36H), 0.87 (t,  $J = 7.2$  Hz, 6H). <sup>13</sup>C NMR (CDCl<sub>3</sub>, ppm):  $\delta$  142.86, 141.37, 139.43, 137.97, 134.26, 130.56, 129.08, 127.79, 126.32, 125.83, 118.00, 32.10, 30.86, 29.84, 29.75, 29.66, 29.52, 22.84, 14.22. Anal. calcd for C<sub>50</sub>H<sub>64</sub>S<sub>4</sub>: C, 75.70; H, 8.13; S, 16.17. Found: C, 75.82; H, 8.03; S, 15.94. MALDI-TOF-MS (dithranol)  $m/z$ : 792.30 (M); calcd for C<sub>50</sub>H<sub>64</sub>S<sub>4</sub> = 792.40

**2,5-Bis(4-dodecyl-5-(naphth-2-yl)thiophen-2-yl)thieno[3,2-*b*]thiophene (1b)** (3.2 g, 67% yield): <sup>1</sup>H NMR (CDCl<sub>3</sub>, ppm)  $\delta$  7.88–7.86 (m, 8H), 7.61–7.58 (m, 2H), 7.54–7.50 (m, 4H), 7.32 (s, 2H), 7.14 (s, 2H), 2.72 (t,  $J = 7.6$  Hz, 4H), 1.72–1.64 (m, 4H), 1.34–1.23 (overlapped peaks 36H), 0.88 (t,  $J = 7.2$  Hz, 6H). <sup>13</sup>C NMR (CDCl<sub>3</sub>, ppm):  $\delta$  140.51, 139.45, 138.78, 137.72, 136.26, 133.86, 132.96, 132.18, 128.54, 128.44, 128.12, 127.66, 126.85, 126.61, 115.84, 32.31, 31.27, 30.01, 29.87, 29.74, 29.29, 23.05, 14.43. Anal. calcd for C<sub>58</sub>H<sub>68</sub>S<sub>4</sub>: C, 77.97; H, 7.67; S, 14.36. Found: C, 77.81; H, 7.83; S, 14.31. MALDI-TOF-MS (dithranol)  $m/z$ : 892.31 (M); calcd for C<sub>58</sub>H<sub>68</sub>S<sub>4</sub> = 892.40

### 2,5-Bis(3-dodecylthiophen-2-yl)thieno[3,2-*b*]thiophene **5**

3-Dodecylthiophene (3 g, 11.95 mmol) was dissolved in dry THF (40 mL) and cooled in an acetone–dry ice bath for 20 min.

*tert*-Butyllithium (1.6 M) (7.47 mL, 11.95 mmol) was then added dropwise and the mixture was allowed to stir for 1 h. Tributyltin chloride (3.24 mL, 11.95 mmol) was then added dropwise and the mixture was allowed to warm to room temperature and stir for 1 h. Meanwhile, in a separate flask, PdCl<sub>2</sub>(PPh<sub>3</sub>)<sub>2</sub> (0.175 g, 0.25 mmol) was dissolved in THF (20 mL) and 2,5-dibromothiopheno[3,2-*b*]thiophene (**4**) (1.50 g, 5 mmol) was added. The tributyl(3-dodecylthiophen-2-yl)stannane (**2**) was transferred into the catalyst–2,5-dibromothiopheno[3,2-*b*]thiophene solution and refluxed for 20 h. The solution was then allowed to cool, quenched with water, and extracted with dichloromethane. The organic layer was separated and dried over MgSO<sub>4</sub>. After solvent removal the crude product was purified by column chromatography over silica gel and recrystallized from dichloromethane–ethanol (2.6 g, 81% yield). <sup>1</sup>H NMR (CDCl<sub>3</sub>, ppm) δ 7.20 (s, 2H), 7.04 (d, *J* = 7.6 Hz, 2H), 6.83 (d, *J* = 7.6 Hz, 2H), 2.59 (t, *J* = 7.6 Hz, 2H), 1.65–1.60 (m, 2H), 1.42–1.26 (overlapped peaks 18H), 0.88 (t, *J* = 7.2 Hz, 3H). Calcd for C<sub>38</sub>H<sub>56</sub>S<sub>4</sub>: C, 71.19; H, 8.80; S, 20.01. Anal. found: C, 70.91; H, 8.66; S, 19.80. MALDI-TOF-MS (dithranol) *m/z*: 640.19 (M); calcd for C<sub>38</sub>H<sub>56</sub>S<sub>4</sub> = 640.30.

### 2,5-Bis(5-bromo-3-dodecylthiophen-2-yl)thieno[3,2-*b*]thiophene **6**

*N*-Bromosuccinimide (0.28 g, 1.56 mmol) was added in portions over 20 min to a solution of **5** (0.5 g, 0.78 mmol) in DMF (20 mL) at 0 °C. After stirring the solution for 3 h at ambient temperature, water (50 mL) was added, and the aqueous layer was extracted with ethyl acetate (50 mL). The organic layer was dried (anhydrous Na<sub>2</sub>SO<sub>4</sub>) and the solvent was removed *in vacuo*. The residue was purified by chromatography on silica gel eluting with hexanes to give **6** (0.56 g, 90% yield). <sup>1</sup>H NMR (CDCl<sub>3</sub>, ppm) δ 7.20 (s, 2H), 6.89 (s, 2H), 2.54 (t, *J* = 7.6 Hz, 4H), 1.62–1.55 (m, 4H), 1.33–1.26 (overlapped peaks 36H), 0.88 (t, *J* = 7.2 Hz, 6H). MALDI-TOF-MS (dithranol) *m/z*: 798.29 (M); calcd for C<sub>38</sub>H<sub>54</sub>S<sub>4</sub>Br<sub>2</sub> = 798.90

### General method for **2a** and **2b**

To a deoxygenated solution of aryl boronic acid **7** [phenyl boronic acid (0.19 g, 1.57 mmol) (**7a**) or 2-naphthyl boronic acid (0.27 g, 1.57 mmol) (**7b**)] and Na<sub>2</sub>CO<sub>3</sub> (20 mL, 2 M), a deoxygenated solution **6** (0.5 g, 0.63 mmol) in toluene (60 mL) and tetrakis(triphenylphosphine palladium(0)) (0.036 g, 0.031 mmol) was added. The reaction mixture was refluxed for 24 h under an argon atmosphere. The cooled solution was poured into water, extracted with dichloromethane and dried over magnesium sulfate. The final solution was purified by column chromatography (silica gel, hexane) and recrystallized from dichloromethane–ethanol to yield **2a** (0.38 g, 77%) as yellow crystals and **2b** (0.41, 73%) as orange crystals.

**2a**: <sup>1</sup>H NMR (CDCl<sub>3</sub>, ppm) δ 7.62 (d, *J* = 8 Hz, 4H), 7.39 (t, *J* = 7.6 Hz, 4H), 7.28 (t, *J* = 7.2 Hz, 2H), 7.18 (s, 2H), 7.01 (s, 2H), 2.64 (t, *J* = 7.6 Hz, 4H), 1.67–1.62 (m, 4H), 1.34–1.25 (overlapped peaks 36H), 0.88 (t, *J* = 7.2 Hz, 6H). <sup>13</sup>C NMR (CDCl<sub>3</sub>, ppm): δ 139.86, 139.20, 138.60, 137.58, 135.73, 134.50, 129.41, 128.73, 127.69, 126.54, 115.58, 32.09, 31.01, 30.54, 29.80, 29.72, 29.62, 28.97, 22.84, 14.23. Anal. calcd for C<sub>50</sub>H<sub>64</sub>S<sub>4</sub>: C, 75.70; H, 8.13; S, 16.17. Found: C, 75.64; H, 8.27; S, 16.06. MALDI-TOF-MS (dithranol) *m/z*: 792.24 (M); calcd for C<sub>50</sub>H<sub>64</sub>S<sub>4</sub> = 792.40

**2b**: <sup>1</sup>H NMR (CDCl<sub>3</sub>, ppm) δ 7.92–7.86 (m, 8H), 7.60–7.58 (d, *J* = 8.4 Hz, 2H), δ 7.52–7.48 (m, 4H), 7.33 (s, 2H), 7.14 (s, 2H), 2.72 (t, *J* = 7.6 Hz, 4H), 1.67–1.60 (m, 4H), 1.32–1.24 (overlapped peaks 36H), 0.88 (t, *J* = 7.2 Hz, 6H). <sup>13</sup>C NMR (CDCl<sub>3</sub>, ppm): δ 140.44, 139.41, 138.84, 137.74, 136.23, 133.78, 132.97, 132.14, 128.56, 128.48, 128.39, 128.10, 127.67, 126.87, 126.63, 115.84, 32.32, 31.28, 30.04, 29.87, 29.75, 29.31, 23.01, 14.50. Calcd for C<sub>58</sub>H<sub>68</sub>S<sub>4</sub>: C, 77.97; H, 7.67; S, 14.36. Found: C, 78.01; H, 7.54; S, 14.43. MALDI-TOF-MS (dithranol) *m/z*: 892.37 (M); calcd for C<sub>58</sub>H<sub>68</sub>S<sub>4</sub> = 892.40

### Scanning tunneling microscopy (STM)

*In situ* STM measurements were performed at the *n*-tetradecane–substrate (liquid–solid) interface at room temperature in constant current mode using a Pico LE SPM system (Molecular Imaging). STM tips were prepared from a Pt–Ir (80 : 20) wire by mechanical cutting. Compounds **1a** and **2a** were dissolved in *n*-tetradecane (*n*-C<sub>14</sub>H<sub>30</sub>, Aldrich, 99.99%) prior to deposition. A droplet of approximately 5 μL of a 0.1 mg mL<sup>−1</sup> solution of the compound was then dropped onto a freshly cleaved HOPG substrate (Goodfellow).

### OFET device performance

Field-effect transistors were made both in bottom-contact (semiconductor deposited above the drain and source electrodes) and top-contact (drain and source deposited above the semiconductor) device geometries by solution deposition. A heavily doped Si wafer was used as a substrate and gate electrode with 100 nm thermally grown SiO<sub>2</sub> serving as a gate dielectric. Before thin film deposition, the Si wafer was cleaned by a piranha solution followed by SC1. For the bottom-contact structure, the gold layer (source and drain) with a thickness of 100 nm was sputter-deposited and patterned by photolithography and lift-off to define the source and drain electrodes. For the top-contact structure, the gold electrodes (source and drain) were thermally evaporated and defined by using a shadow mask with a film thickness of 40 nm.

All transistors were characterized under a N<sub>2</sub> environment. From the electrical transfer characteristics (*I*<sub>d</sub>–*V*<sub>g</sub>), the parameters such as carrier mobility, threshold voltage, current on/off ratio, and subthreshold swing were extracted. The carrier mobility was calculated from the saturation regime at a drain–source voltage of −30 V and a gate–source voltage of −30 V. In order to minimize the leakage current, every device was isolated by scratching a trench around the active device area with a probe tip to remove the organic semiconductor from the trench.<sup>26</sup>

### Solution processed OFET

All solution processed devices using bottom-contact geometry, in general, showed lower charge carrier mobility than those using the top-contact geometry. Other researchers also reported this phenomenon for other semiconductive materials; this could be attributed to the small charge injection areas and poor ordering of the organic semiconductor on the electrodes in the bottom-contact geometry.<sup>29</sup>

The bottom-contact devices have a channel length of 11120 μm and a channel width of 30 μm. The smoothest and most

continuous film was obtained by spin coating from toluene solutions. Other solvents like THF, chloroform, chlorobenzene and dichlorobenzene resulted in poor-connectivity films observed by optical microscope. Various concentrations ranging from 0.05 wt% to 0.5 wt% were also tested since it was reported that generally the solubility and solution concentration is crucial to the quality of the films.<sup>30</sup> The uniform and good-connectivity film was only obtained from the toluene solution with the highest concentration of 0.5 wt%. Lower concentrations resulted in uneven films, distinguishable by eye, or islands of crystalline materials by optical microscope. Different annealing temperatures from 100 °C to 180 °C, annealing times from 15 to 40 min and annealing atmospheres, both under vacuum and N<sub>2</sub>, were also studied. It was found that higher annealing temperatures ( $T_{\text{anneal}} > 120$  °C) resulted in poor device performance and there was no obvious enhancement in device performance through longer annealing time. Vacuum oven annealing and cooling down overnight resulted in a better performance, since the cooling rate played an important role in improving the film quality. Studies showed that slower cooling rates gave a better molecular ordering, and hence higher device performance.<sup>31</sup>

## Acknowledgements

This work was supported by an A\*STAR grant (Research Grant No. 052 117 0032).

## References

- (a) K. Takimiya, H. Ebata, K. Sakamoto, T. Izawa, T. Otsubo and Y. Kunugi, *J. Am. Chem. Soc.*, 2006, **128**, 12604; (b) G. Horowitz and P. Delannoy, in *Handbook of Oligo- and Polythiophenes*, ed. D. Fichou, Wiley-VCH, Weinheim, Germany, 1999; (c) Y. Li, Y. Wu, P. Liu, M. Birau, H. Pan and B. S. Ong, *Adv. Mater.*, 2006, **18**, 3029; (d) M. Mushrush, A. Facchetti, M. Lefenfeld, H. E. Katz and T. J. Marks, *J. Am. Chem. Soc.*, 2003, **125**, 9414.
- (a) X. Zhang and A. J. Matzger, *J. Org. Chem.*, 2003, **68**, 9813; (b) Z. Bao, *Adv. Mater.*, 2000, **12**, 227; (c) G. Barbarella, L. Favaretto, G. Sotgiu, M. Zambianchi, V. Fattori, M. Cocchi, F. Cacialli, G. Gigli and R. Cingolani, *Adv. Mater.*, 1999, **11**, 1375; (d) U. Mitschke and P. Bäuerle, *J. Chem. Soc., Perkin Trans. 1*, 2001, 740; (e) V. Dediu, M. Murgia, F. C. Matacotta, C. Taliani and S. Barbanera, *Solid State Commun.*, 2002, **122**, 181; (f) K. Ogawa and S. C. Rasmussen, *J. Org. Chem.*, 2003, **68**, 2921.
- C. Vidélot-Ackermann, J. Ackermann, H. Brisset, K. Kawamura, N. Yoshimoto, P. Raynal, A. El Kassmi and F. Fages, *J. Am. Chem. Soc.*, 2005, **127**, 16346.
- H. Sirringhaus, N. Tessler, D. S. Thomas, P. J. Brown and R. H. Friend, *Adv. Solid State Phys.*, 1999, **39**, 101, and in the Merck patent, EP 1 279 689 A2, 2003.
- J. Nakayama, H. B. Dong, K. Sawada, A. Ishii and S. Kumakura, *Tetrahedron*, 1996, **52**, 471.
- (a) X. Zhang, M. Kohler and A. J. Matzger, *Macromolecules*, 2004, **37**, 6306; (b) X. Zhang, J. P. Johnson, J. W. Kampf and A. J. Matzger, *Chem. Mater.*, 2006, **18**, 3470.
- W. H. Tang, L. Ke, L. W. Tan, T. T. Lin, T. Kietzke and Z.-K. Chen, *Macromolecules*, 2007, **40**, 6164.
- U. Tokiyoshi and T. Shizuo, *J. Appl. Phys.*, 2007, **101**, 054517.
- E. Lim, B. J. Jung and H. K. Shim, *Macromolecules*, 2003, **36**, 4288.
- H.-S. Kim, Y.-H. Kim, T.-H. Kim, Y.-Y. Noh, S. Pyo, M. H. Yi, D.-Y. Kim and S.-K. Kwon, *Chem. Mater.*, 2007, **19**, 3561.
- Y.-Y. Noh, R. Azumi, M. Goto, B.-J. Jung, E. H. Lim, H.-K. Shim, Y. Yoshida, K. Yase and D.-Y. Kim, *Chem. Mater.*, 2005, **17**, 3861.
- I. McCulloch, M. Heeney, C. Bailey, K. Genevicius, I. MacDonald, M. Shkunov, D. Sparrowe, S. Tierney, R. Wagner, W. Zhang, M. L. Chabynyc, R. J. Kline, M. D. McGehee and M. F. Toney, *Nat. Mater.*, 2006, **5**, 328.
- (a) D. R. Rutherford, J. K. Stille, C. M. Elliott and V. R. Reichert, *Macromolecules*, 1992, **25**, 2294; (b) C. Taliani, R. Zamboni, R. Danieli, P. Ostojia, W. Porzio, R. Lazzaroni and J. L. Bredas, *Phys. Scr.*, 1989, **40**, 781; (c) R. Danieli, C. Taliani, R. Zamboni, G. Giro, M. Biserni, M. Mastragostino and A. Testoni, *Synth. Met.*, 1986, **13**, 325.
- (a) H. Tian, J. Shi, D. Yan, L. Wang, Y. Geng and F. Wang, *Adv. Mater.*, 2006, **18**, 2149; (b) S. Mohapatra, B. T. Holmes, C. R. Newman, C. F. Prendergast, C. D. Frisbie and M. D. Ward, *Adv. Funct. Mater.*, 2004, **14**, 605; (c) M. Mushrush, A. Facchetti, M. Lefenfeld, H. E. Katz and T. J. Marks, *J. Am. Chem. Soc.*, 2003, **125**, 9414.
- K. R. Radke, K. Ogawa and S. C. Rasmussen, *Org. Lett.*, 2005, **7**, 5253.
- Y. Wu, Y. Li, S. Gardner and B. S. Ong, *J. Am. Chem. Soc.*, 2005, **127**, 614.
- Y. Sun, Y. Ma, Y. Liu, Y. Lin, Z. Wang, Y. Wang, C. Di, K. Xiao, X. Chen, W. Qiu, B. Zhang, G. Yu, W. Hu and D. Zhu, *Adv. Funct. Mater.*, 2006, **16**, 426.
- (a) N. Katsonis, A. Marchenko and D. Fichou, *J. Am. Chem. Soc.*, 2003, **125**, 13682; (b) L. Piot, J. Wu, A. Marchenko, K. Mullen and D. Fichou, *J. Am. Chem. Soc.*, 2005, **127**, 16245; (c) A. Nion, P. Jiang, A. Popoff and D. Fichou, *J. Am. Chem. Soc.*, 2007, **129**, 2450; (d) A. Popoff and D. Fichou, *Colloids Surf., B*, 2008, **63**, 153.
- (a) P. Keg, A. Lohani, D. Fichou, Y. M. Lam, Y. Wu, B. S. Ong and S. G. Mhaisalkar, *Macromol. Rapid Commun.*, 2008, **29**, 1197; (b) A. Dell'Aquila, F. Marinelli, J. Tey, P. Keg, Y. M. Lam, O. L. Kapitanchuk, P. Mastrorilli, C. F. Nobile, A. Marchenko, D. Fichou, S. G. Mhaisalkar, G. P. Suranna and L. Torsi, *J. Mater. Chem.*, 2008, **18**, 786; (c) E. Mena-Osteritz, *Adv. Mater.*, 2002, **14**, 609.
- (a) J. P. Rabe and S. Buchholz, *Science*, 1991, **253**, 424; (b) D. M. Cyr, B. Venkataraman, G. W. Flynn, A. Black and G. M. Whitesides, *J. Phys. Chem.*, 1996, **100**, 13747.
- (a) M. M. S. Abdel-Mottaleb, G. Gotz, P. Kilickiran, P. Bauerle and E. Mena-Osteritz, *Langmuir*, 2006, **22**, 1443; (b) R. Azumi, G. Gotz, T. Debaerdemaeker and P. Bauerle, *Chem.-Eur. J.*, 2000, **6**, 735; (c) R. Azumi, G. Gotz and P. Bauerle, *Synth. Met.*, 1999, **101**, 569; (d) T. Kirschbaum, R. Azumi, E. Mena-Osteritz and P. Bauerle, *New J. Chem.*, 1999, 241; (e) R. Stecher, B. Gompf, J. S. R. Munter and F. Effenberger, *Adv. Mater.*, 1999, **11**, 927; (f) A. Stabel and J. P. Rabe, *Synth. Met.*, 1994, **67**, 47; (g) P. Bauerle, T. Fischer, B. Bidlingmeier, A. Stabel and J. P. Rabe, *Angew. Chem., Int. Ed.*, 1995, **34**, 303.
- W. Pisula, Z. Tomovic, C. Simpson, M. Kastler, T. Pakula and K. Müllen, *Chem. Mater.*, 2005, **17**, 4296.
- M. L. Chabynyc, M. F. Toney, R. J. Kline, I. McCulloch and M. Heeney, *J. Am. Chem. Soc.*, 2007, **129**, 3226.
- (a) W. Pisula, M. Kastler, D. Wasserfallen, T. Pakula and K. Müllen, *J. Am. Chem. Soc.*, 2004, **126**, 8074; (b) W. Pisula, F. Dierschke and K. Müllen, *J. Mater. Chem.*, 2006, **16**, 4058; (c) W. Pisula, Z. Tomovic, M. Wegner, R. Graf, M. J. Pouderoijen, E. W. Meijer and A. P. H. J. Schenning, *J. Mater. Chem.*, 2008, **18**, 2968; (d) H. Shen, K.-U. Jeong, H. Xiong, M. J. Graham, S. Leng, J. X. Zheng, H. Huang, M. Guo, F. W. Harris and S. Z. D. Cheng, *Soft Matter*, 2006, **2**, 232.
- J. L. Hutter and J. Bechhoefer, *J. Cryst. Growth*, 2000, **217**, 332.
- H. Meng, J. Zheng, A. J. Lovinger, B. C. Wang, P. G. Van Patten and Z. Bao, *Chem. Mater.*, 2003, **15**, 1778.
- P. Bauerle, F. Pfau, H. Schlupp, F. Wurthner, K.-U. Gaudl, M. B. Carot and P. Fischert, *J. Chem. Soc., Perkin Trans. 2*, 1993, 489.
- L. S. Fuller, B. Iddon and K. A. Smith, *J. Chem. Soc., Perkin Trans. 1*, 1997, 3465–3470.
- S. A. Ponomarenko, S. Kirchmeyer and A. Elschner, *Chem. Mater.*, 2006, **18**, 579–586.
- C. Reese, M. Roberts, M. Ling and Z. Bao, *Mater. Today*, 2004, **7**, 20–27.
- N. Zhao, G. A. Botton, S. Zhu, A. Duft, B. S. Ong, Y. Wu and P. Liu, *Macromolecules*, 2004, **37**, 8307.